THE JOURNAL OF PHYSICAL CHEMISTRY B

Article

pubs.acs.org/JPCB

Insights on How the Activity of an Endoglucanase Is Affected by Physical Properties of Insoluble Celluloses

Juliano Bragatto, Fernando Segato, Junio Cota, Danilo B. Mello, Marcelo M. Oliveira, Marcos S. Buckeridge, Fabio M. Squina, and Carlos Driemeier*

Laboratório Nacional de Ciência e Tecnologia do Bioetanol, CTBE, Caixa Postal 6170, 13083-970 Campinas, São Paulo, Brazil

Supporting Information

ABSTRACT: Cellulose physical properties like crystallinity, porosity, and particle size are known to influence cellulase activity, but knowledge is still insufficient for activity prediction from such measurable substrate characteristics. With the aim of illuminating enzyme–substrate relationships, this work evaluates a purified hyperthermophilic endo-1,4-beta-glucanase (from *Pyrococcus furiosus*) acting on 13 celluloses characterized for crystallinity and crystal width (by X-ray diffraction), wet porosity (by thermoporometry), and particle size (by light scattering). Activities are analyzed by the Michaelis–Menten kinetic equation, which is justified by low enzyme–substrate affinity. Michaelis–Menten coefficients K_m and k_{cat} are reinterpreted in the context of heterogeneous cellulose hydrolysis. For a set of as-received and milled microcrystalline celluloses, activity is successfully described as a function of accessible substrate concentration, with accessibility proportional to K_m^{-1}. Accessibility contribution from external particle areas, pore areas, and crystalline packing are discriminated to have comparable magnitudes, implying that activity prediction demands all these substrate properties to be considered. Results additionally suggest that looser crystalline packing increases the lengths of released cello-oligomers as well as the maximum endoglucanase specific activity (k_{cat}).

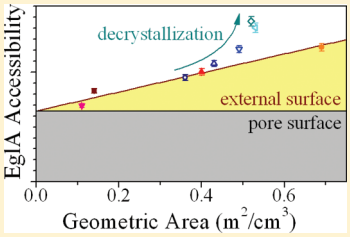

1. INTRODUCTION

Cellulosic biomass will substitute a significant share of fossil resources currently used for materials, chemicals, and fuels. Enzymatic saccharification is one of the most studied strategies to convert the recalcitrant and insoluble cellulosic feedstocks into simple sugars that are reactive soluble intermediates.[1,2] A major use for glucose obtained from cellulose hydrolysis is its fermentation to ethanol, which is already a widespread transportation fuel.[3]

Three different types of cellulases are involved in cellulose hydrolysis: endoglucanases (EC 3.2.1.4), cellobiohydrolases (EC 3.2.1.91, EC 3.2.1.176), and β-glucosidases (EC 3.2.1.21). Current paradigm states that endoglucanases randomly hydrolyzes β-1,4 bonds within cellulose amorphous regions. At the chain ends created by endoglucanases, cellobiohydrolases can start the processive deconstruction of crystalline cellulose, releasing soluble cellobiose that β-glucosidases hydrolyze to glucose.[4−6]

As reviewed extensively by many authors,[5−9] enzymatic hydrolysis of cellulosic substrates is complex. There are synergies between the different types of enzymes. Reactions are inhibited by accumulation of hydrolysis products. Realistic cellulosic resources have, in addition to cellulose, hemicellulose and lignin; these other components compete for enzyme adsorption, hinder access to cellulose, and ultimately require other enzymes such as xylanases and ligninases. Finally, cellulosic substrates are insoluble in water, implying heterogeneous reactions that depend on substrates' tridimensional organization.

The complexity from substrate structure is partly summarized in the concept of accessibility.[10,11] This concept highlights that only a fraction of the substrate mass is actually reachable by cellulases, whose movements are restricted by their sizes of about 5 nm. Measurable substrate properties like surface areas and porosity[12−14] have been proposed to modulate accessibility and, in this way, affect hydrolysis rate.

There is also the issue of cellulose crystallinity.[7,15,16] Understanding its effect on hydrolysis rates faces two fundamental challenges. First, cellulose crystallinity measurements are somewhat ambiguous,[16] and unfortunately, careless crystallinity measurements are common. For instance, X-ray diffraction (XRD) factors significant for cellulose crystallinity measurements[17] are often neglected. Second, there are cellulases specialized in crystalline as well as in noncrystalline cellulose.[5] Hence, relationships between substrate crystallinity and hydrolysis rate are a function of the cellulase system.

Against this background of complexity, this article investigates enzymatic hydrolysis in rather simple systems with the aim of illuminating mechanisms in complex realistic systems. Hydrolysis was performed with a single purified cellulase, the hyperthermophilic endo-1,4-beta-glucanase from *Pyrococcus furiosus* (EglA).[18,19] EglA activities were compared on 13 insoluble cellulosic substrates with extensive characterization of physical properties (crystallinity, crystal width, wet porosity, and particle size). Activities were analyzed by Michaelis–

Received: March 6, 2012
Revised: May 2, 2012
Published: May 11, 2012

Menten kinetic equation, whose parameters K_m and k_{cat} were reinterpreted in the context of heterogeneous cellulose hydrolysis. For a set of as-received and milled microcrystalline celluloses, activity contributions from external particle areas, pore areas, and decrystallization could be discriminated to have similar magnitudes, implying that activity prediction demands all these substrate properties to be considered.

2. MATERIALS AND METHODS

2.1. Cellulosic Substrates. The following cellulosic substrates were acquired from Sigma-Aldrich (catalog code in parentheses) in September 2010: Fluka cellulose (22183), Sigmacell type 20 (S3504), Sigmacell type 50 (S5504), Avicel PH-101 (11365), Sigmacell type 101 (S6790), and α-cellulose (C8002). This study also included a bleached eucalyptus kraft pulp and a sugar cane bagasse pulp produced in a 1:1 mixture of 8.74 M glacial acetic acid and 21.6 M hydrogen peroxide at 60 °C for 48 h. All substrates were handled in the laboratory atmosphere, acquiring ~5−10% equilibrium moisture contents. These substrates are henceforth named Fluka, S20, S50, Avicel, S101, Alpha, E_{pulp}, and B_{pulp}, respectively.

Avicel was processed in a Fritsch Pulverisette 14 centrifugal mill at 20.000 rpm, 0.08 mm mesh sieving ring, with milling cycles of 3 min. In this process, particles are comminuted by impact with the rotating ribs as well as by shear and friction between the sieving ring and the rotor ribs. In addition to as-received Avicel, milled Avicel was prepared by performing 1 to 5 sequential milling cycles. E_{pulp} and B_{pulp} were also submitted to one milling cycle (same conditions) to produce particulates suitable for the enzymatic hydrolysis.

2.2. Substrate Composition. Cellulose and xylan contents in the cellulosic substrates were determined following standard protocol.[20] Representative samples of 100 mg were hydrolyzed in two steps: 72% H_2SO_4 for 1 h at 30 °C, followed by dilution to 2.5% H_2SO_4 and an additional 1 h at 121 °C. Samples were then quenched in ice and filtered. Cellobiose, glucose, and xylose concentrations in the filtrates were determined by high performance anion exchange chromatography (HPAE) with a Dionex ICS-3000 system. Concentrations of cellobiose and glucose were converted to dry-mass percentage (%DM) of cellulose, and concentrations of xylose were converted to %DM of xylan.

2.3. Substrate Physical Properties. A first glance on particulate properties was obtained by scanning electron microscopy (SEM) performed in a JEOL JSM-5900LV instrument operated with 15 kV accelerating voltage, 15 cm working distance, and detection of secondary electrons. Samples were stick on stubs and coated with gold.

Particle size distributions were determined by light scattering using a Beckman Coulter LS13320 instrument with Tornado Dry Powder module, as detailed elsewhere.[21] The Mie light-scattering model was employed, inputting cellulose refraction index $n = 1.54$. The model converts measured light scattering to particle size distributions, given as volume percentages $\%v_i$ distributed in channels of equivalent particle diameter d_i.

From each particle size distribution, a geometric surface area S_g was calculated (in units of m^2/cm^3) by

$$S_g = \sum_i \frac{6}{d_i}\frac{\%v_i}{100} \quad (1)$$

which is the summation of surface-to-volume ratio for spheres ($6/d_i$) weighted by the volume fractions ($\%v_i$ /100) associated with each d_i. Hence, strictly speaking, S_g is the specific surface area from an ensemble of spheres with size distribution $\%v_i$ (d_i). Since realistic particles are not spheres, measured particle size distributions and S_g calculated from them are not fully quantitative parameters. Nevertheless, they still provide correct scaling with particle sizes.

Wet porosity was measured by thermoporometry with differential scanning calorimetry (TP-DSC) in a TA Instruments Q200 system with autosampler and RCS90 cooling unit. Our procedure[22] follows Park et al.[23] but with sample freezing temperature extended to −70 °C and corrections added to estimations of sample heat capacity. TP-DSC is based on the melting temperature depression ΔT of ice confined in pores. Pore volumes are calculated from measured heats of ice melting, while pore diameters x are estimated by $x = -2K_c/\Delta T$ (with K_c = 19.8 nm), which is a concise form of the Gibbs−Thomson equation. Reported data is the cumulative freezing pore water (in units of g of pore ice per g of dry matter) as a function of pore diameter x.

From each TP-DSC pore size distribution, specific pore area S_p was calculated (in units of m^2/g) by

$$S_p = \int \frac{2}{x\rho_{ice}} dM \quad (2)$$

where ρ_{ice} = 0.917 g/cm^3 is ice density, and dM is the differential molten ice mass. The integral was restricted to pores of diameter $x > 10$ nm, which estimates with some margin the areas accessible to enzymes of ~5 nm. Derivation of eq 2 considers ice melting governed by energy barrier removal, which is a simplification of melting with interplay between equilibrium and barrier removal.[22]

XRD was performed as in previous studies,[17,24] using a Rigaku ultraX-18HF rotating anode generator with monochromated Cu Kα radiation (wavelength λ = 1.54 Å) and mar345 image plate detector. Two-dimensional diffraction patterns were acquired and analyzed by the Rietveld method, using the MAUD program[25] with description of preferred crystal orientation. Crystallinity and crystal width were determined from XRD. Crystallinity was defined as %DM crystal content, and its determination included correction of experimental data, modeling of crystalline signal, integration of intensity in a standard interval, and accounting intensities from blank, adsorbed moisture, and incoherent scattering.[17] Crystal width was derived from the Scherrer equation applied to the width of 200 diffraction peaks, as implemented in the Rietveld analysis software. The robustness of this XRD method was previously demonstrated by its application to a wide spectrum of celluloses.[24]

2.4. Enzyme Production, Purification, and Modeling. EglA belongs to glycosyl hydrolase family 12[26] and lacks carbohydrate binding module. The gene encoding EglA, as derived from genomic DNA, was analyzed by the SignalP (Center for Biological Sequence Analyzes) program and the signal peptide sequence was removed. The gene was amplified by standard PCR method to clone the full-length enzyme. Amplification used the primer set 5′-TATA**GCTAGC**TCCT-CAACCCCCCCTCAAACGACACTTAG-3′ (forward) and 5′-T A T A **G G A T C C** G G G A G A T C A G G G G A C G A T-CAAGTGGGGT-3′ (reverse). These primers contain NheI and *Bam*HI restriction sites flanking the respective primer sequence (in bold) to orientate a gene cloning segment into the pET28a (Novagen) vector.

dx.doi.org/10.1021/jp3021744 | J. Phys. Chem. B 2012, 116, 6128−6136

The resulting enzyme, which has a 6× HisTag tail, was purified by Ni^{2+}-chelating affinity followed by size-exclusion chromatography.[27] Concentration of the purified enzyme was determined by the Bradford method.[28] Enzyme purity was verified by sodium dodecyl sulfate-polyacrylamide gel electrophoresis.

EglA protein sequence was modeled on Swiss-prot[29] against the endo-1,4-beta-glucanase from *Thermotoga maritima* protein structure[30] (also belonging to glycosyl hydrolase family 12), showing 77% similarity on structures. On the basis of this modeling, EglA (34 kDa) has a size of 6.5 × 5.5 × 6.3 nm^3 and active site inside a cleft.

2.5. Enzymatic Hydrolysis. Enzymatic hydrolysis was performed in 2 mL sealed microtubes shaken at 1000 rpm in an Eppendorf 21516-172 Thermomixer. This mixing conditions suspended cellulose particulates in a solution prepared with 1 mL of 50 mmol/L citrate/phosphate buffer.[31] Target solid masses were 10, 30, 50, or 100 mg. Actual solid masses were determined gravimetrically, correcting for moisture contents in the solids. Hydrolysis conditions were 0.023 mg of EglA, 15 h, 85 °C, and pH 7.5. This temperature and pH was optimal for hydrolysis of carboxymethyl cellulose, as determined by testing the range 70−90 °C × pH 4.0−9.0. All hydrolyses reactions were done in triplicates.

Reducing sugar concentration in supernatants from enzymatic hydrolysis was determined by dinitrosalicylic acid assay (DNS),[32] measuring absorbance at 540 nm (in a Tecan Infinite M200 instrument) and referencing to calibration curves from glucose solutions. To calculate specific enzymatic activities (in units of μmol h^{-1} mg^{-1}), reducing sugar concentration (in units of mol/L) was multiplied by solution volume (1 mL) and divided by hydrolysis time (15 h) and enzyme loading (0.023 mg). To convert activity to hydrolyzed mass, one notes that, with the aforementioned conditions, 1 mg of cellulose converted to glucose corresponds to an activity of 17.9 μmol h^{-1} mg^{-1}. HPAE was also employed to discriminate hydrolysate concentrations of glucose, cellobiose, xylose, arabinose, and galactose, but this HPAE analysis was limited to supernatants from hydrolysis with ∼10 mg of solids.

2.6. Data Analysis. Measured specific enzymatic activity Y as a function of substrate concentration $[S]$ was analyzed with the equation

$$Y = \frac{k_{cat}[S]}{K_m + [S]} \quad (3)$$

which is the Michaelis−Menten kinetics equation,[33] with fitting coefficients K_m and k_{cat}. Fitting was done by precision-weighted least-squares, using the linearized coordinates $[S]/Y \times [S]$. Substrate sets were fitted with a K_m for each substrate and a single k_{cat} for the whole set. With these fitting conditions, a set of $Y \times [S]$ curves collapse into a single curve with K_m^{-1} $[S]$ in the abscissa.

All reported uncertainties are 1σ precisions. For enzymatic activities analyzed by eq 3, precisions were calculated as the standard deviation of the mean (from triplicate measurements). Nevertheless, a lower limit of 2% relative precision was imposed to avoid fitting bias from measurements presenting uncommon repeatability within the triplicates.

3. RESULTS AND DISCUSSIONS

3.1. Substrate Properties. The cellulosic substrates of the present study were grouped according to shared characteristics.

Table 1. Composition of Cellulosic Substrates

group	substrate	cellulose (%DM)	xylan (%DM)
MCC	Fluka	99.8 ± 0.2	0.17 ± 0.01
	S20	99.8 ± 0.3	0.20 ± 0.03
	S50	97.5 ± 0.5	2.49 ± 0.49
	Avicel	99.8 ± 0.1	0.16 ± 0.01
FBR	S101	80.0 ± 1.3	19.9 ± 1.2
	Alpha	78.6 ± 0.8	21.5 ± 0.8
	E_{pulp}	83.4 ± 0.9	16.7 ± 0.8
	B_{pulp}[a]	81.4 ± 1.8	17.1 ± 0.3

[a] B_{pulp} has ∼1% arabinose.

Table 1 shows that substrates from one group, named microcrystalline celluloses (MCC), were almost 100% cellulose, with xylan contents below 3%. However, substrates from another group, named fibers (FBR), have 17−21% xylan. SEM images evidence that substrates from the FBR group (Figure 1e−h) have particles with high aspect ratios; the exception is S101, whose particles have modest aspect ratios (Figure 1e) comparable to those from MCC group (Figure 1a−d). Nevertheless, S101 was still included in the FBR group because of its higher xylan content.

Figure 2 presents wet porosity from MCC and FBR groups, as well as from Avicel submitted to 1−5 sequential milling cycles, which compose the milled-Avicel (MAV) group. Wet porosities from MCC (Figure 2a) and MAV (Figure 2b) groups are equal within experimental precision. However, substrates from the FBR group are generally more porous than those from MCC and MAV, and porosity varies within the FBR group (Figure 2c). These comparisons can also be made based on pore areas S_p presented in Table 2.

Unimodal particle size distributions are observed for substrates from MCC (Figure 3a) and MAV (Figure 3b) groups, with notable differences in particle sizes as well as in geometric areas S_g (see Table 2). Multimodal particle size distributions, which are typical of fibrous materials,[21] are observed for the FBR group (Figure 3c). As for the images of Figure 1, the exception in the FBR group is S101, whose particle size distribution is qualitatively comparable to those from MCC and MAV groups.

Geometric specific areas (S_g) reported in Table 2 are derived exclusively from particle size distributions. They represent particle external surface areas. Their units can be converted from m^2/cm^3 to m^2/g dividing by particulate envelope densities, which are ∼1.5 g/cm^3 for MCC group (measured as in ref 21). Wet pore areas from TP-DSC are substantially higher than geometric areas (see Table 2), suggesting that wet pores may dominate enzyme accessibility. External areas are, however, generally accessible from the outside of particles, which is not assured for internal pore areas.

Considering precisions in XRD parameters, crystallinity and crystal width (Table 2) are equal within the MCC group, with a possible exception of slightly more crystalline S50. Sequential Avicel milling (MAV group) gradually decreases crystallinity and crystal width, but these effects on crystals are limited. Within the FBR group, crystallinity and crystal width are generally lower than that within MCC and MAV groups, except for the high crystallinity of E_{pulp}. Moreover, there are significant variations in crystallinity and crystal width across the FBR group.

XRD parameters are sample averages. Therefore, observed milling-induced decrystallization and crystal thinning (see MAV

dx.doi.org/10.1021/jp3021744 | J. Phys. Chem. B 2012, 116, 6128−6136

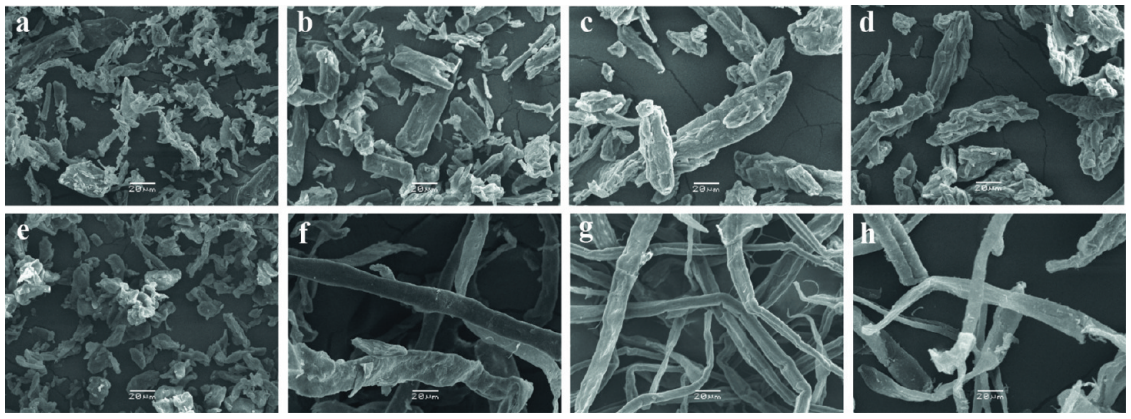

Figure 1. Micrographs from (a) Fluka, (b) S20, (c) S50, (d) Avicel, (e) S101, (f) Alpha, (g) E_{pulp}, and (h) B_{pulp}.

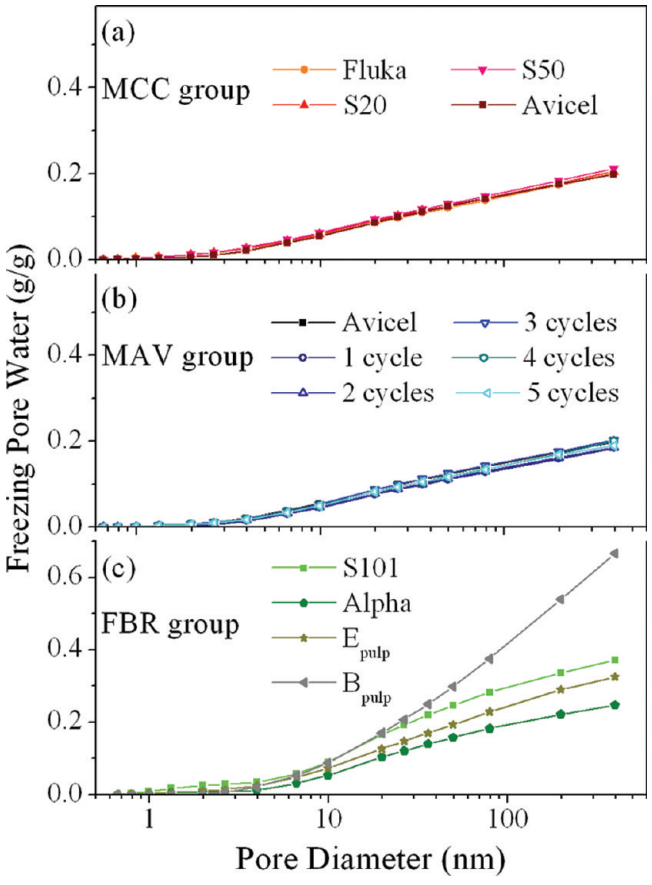

Figure 2. Cumulative pore size distributions determined by thermoporometry for substrates from (a) MCC, (b) MAV, and (c) FBR groups.

group in Table 2) are averages of phenomena likely concentrated at particle surfaces, where milling forces act. Regarding crystallinity uncertainties, 1σ precisions are as good as indicated in Table 2, while accuracy, estimated in several percent, is limited by the peak profiles used to model XRD patterns.[17,24] Taking this accuracy into account, substrates have cellulose content (Table 1) significantly higher than crystallinity (Table 2), indicating that substrates have a significant fraction of noncrystalline cellulose. An exception is E_{pulp}, whose noncrystalline cellulose content is not assured from such comparison.

Substrate properties are summarized as follows. Within the MCC group, variations are concentrated in geometric areas. The MAV group also presents variations in geometric areas, but there is also gradual reduction in crystallinity and crystal width. The FBR group, however, presents highly variable substrate physical properties, with notable differences in particle size and shape, wet porosity, XRD parameters, and surface areas.

3.2. Enzymatic Hydrolysis. Figure 4 presents the molar concentrations of sugars released by enzymatic hydrolysis performed with substrate concentrations of ~10 mg/mL (data from MCC and FBR groups). Molar concentrations of reducing sugars determined by DNS are compared to molar concentrations of glucose and cellobiose determined by HPAE. For samples of higher crystallinity (S20, S50, Avicel, and E_{pulp}; see Table 2), molar concentrations of reducing sugars (by DNS) are only slightly higher than molar concentrations of glucose plus cellobiose (by HPAE). This difference is primarily attributable to DNS overestimation of molar concentrations due to cellobiose, as hydrolysis may take place during DNS assay.[34,35] Hence, for the celluloses of higher crystallinity, glucose and cellobiose are the primary products of EglA action. For samples of lower crystallinity (S101, Alpha, and B_{pulp}; see Table 2), the differences between DNS and HPAE concentrations are higher, indicating the release of larger cellodextrins in addition to glucose and cellobiose. Released arabinose, galactose, and xylose (as verified by HPAE) were below 3% of the released glucose.

Figure 5 shows enzymatic activities (from DNS) as a function of substrate concentration. Hydrolysis yields were limited to ~1% of initial solid masses (see conversion factor in section 2.5), implying minor product inhibition and minor substrate evolution during hydrolysis. Within the MCC group (variability concentrated in geometric areas), there is higher activity (see Figure 5a) for substrates with larger areas (see Table 2). Within the MAV group, there is gradual increase in activity (see Figure 5b) for additional milling cycles. Within the FBR group, activities (see Figure 5c) correlate negatively with crystallinity and crystal width, and positively with geometric and pore areas (see Table 2). In the next sections, activity and substrate properties will be compared in more detail.

3.3. Accessibility Factors. Cellulase activity is usually modeled based on the Langmuir adsorption equation.[5,6] However, under the condition of low enzyme−substrate affinity, the Langmuir equation straightforwardly leads to the Michaelis−Menten equation. In the present work, low enzyme−substrate affinity is a consequence of high temperature

dx.doi.org/10.1021/jp3021744 | J. Phys. Chem. B 2012, 116, 6128−6136

Table 2. X-ray Diffraction (XRD) Parameters and Specific Surface Areas from Cellulosic Substrates

		XRD parameters		specific areas	
group	substrate	crystallinity (%DM)	crystal width (nm)	geometric (m^2/cm^3)	pores (m^2/g)
MCC	Fluka	81 ± 2	6.15 ± 0.05	0.69 ± 0.01	9.2 ± 0.2
	S20	78 ± 2	6.15 ± 0.05	0.40 ± 0.01	9.5 ± 0.4
	S50	85 ± 2	6.22 ± 0.05	0.11 ± 0.01	9.7 ± 0.2
	Avicel	80 ± 2	6.10 ± 0.05	0.14 ± 0.01	9.8 ± 0.2
MAV	1 cycle	77 ± 2	5.96 ± 0.05	0.36 ± 0.01	9.3 ± 0.4
	2 cycles	76 ± 2	5.94 ± 0.05	0.43 ± 0.01	9.4 ± 0.4
	3 cycles	76 ± 2	5.90 ± 0.05	0.49 ± 0.01	10.1 ± 0.4
	4 cycles	75 ± 2	5.88 ± 0.05	0.52 ± 0.01	9.7 ± 0.4
	5 cycles	73 ± 2	5.84 ± 0.05	0.53 ± 0.01	9.7 ± 0.4
FBR	S101	49 ± 4	3.20 ± 0.40	0.54 ± 0.01	21.8 ± 0.3
	Alpha	56 ± 2	4.50 ± 0.10	0.15 ± 0.01	14.5 ± 0.4
	E_{pulp}	84 ± 5	5.61 ± 0.05	0.25 ± 0.01	16.8 ± 0.9
	B_{pulp}	65 ± 3	3.75 ± 0.20	0.25 ± 0.01	30.5 ± 1.2

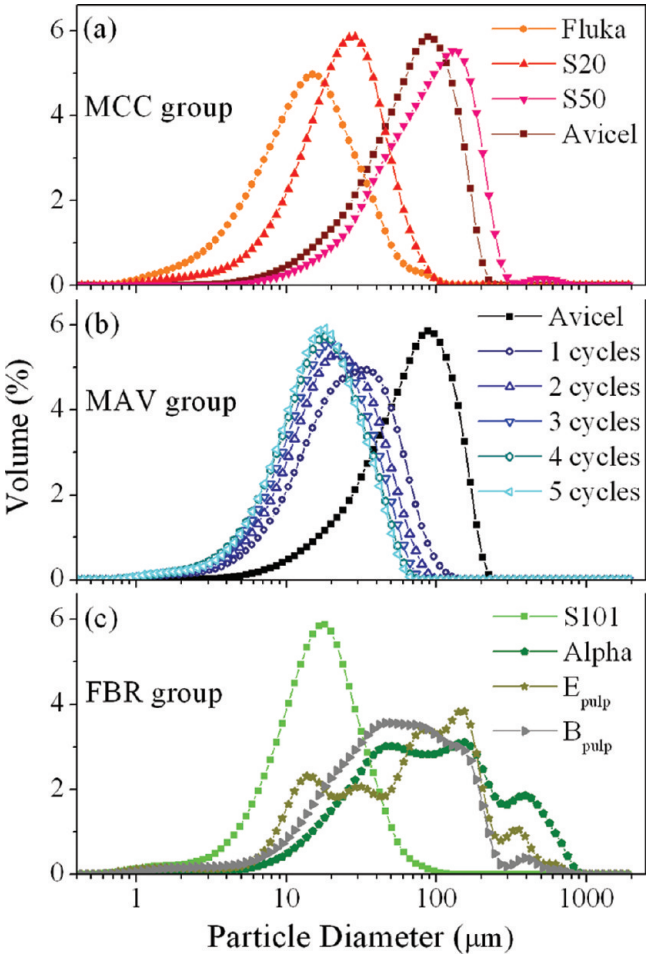

Figure 3. Particle size distributions for substrates from (a) MCC, (b) MAV, and (c) FBR groups.

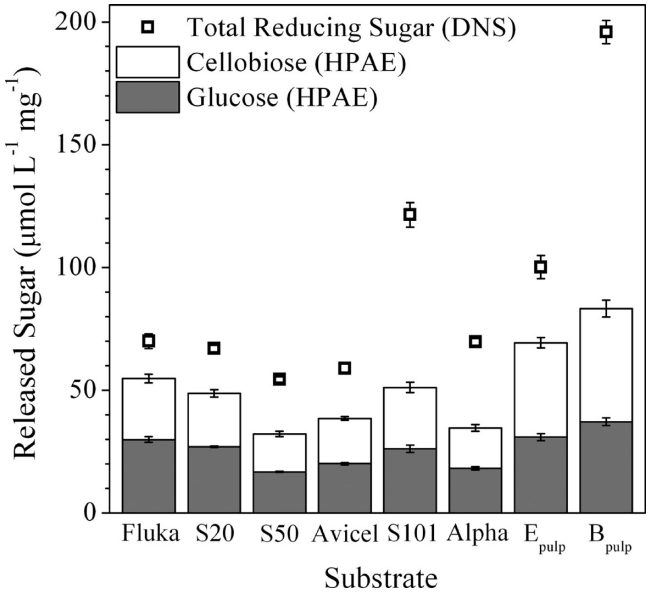

Figure 4. Concentrations of sugars (in units of μmol L^{-1} per mg of substrate) released by enzymatic hydrolysis with substrate concentrations of ~10 mg/mL.

of hydrolysis and EglA lacking carbohydrate binding module. In the Supporting Information, the Michaelis–Menten equation is derived from the Langmuir equation, and the low-affinity limit is verified for the experimental conditions of the present work. For a more detailed mathematic treatment of enzymatic hydrolysis of cellulose, see refs 36 and 37.

Application of the Michaelis–Menten kinetics equation to insoluble substrates must consider that only a fraction of the substrate mass is actually accessible to enzymes. Therefore, instead of analyzing enzyme activity as a function of substrate concentration $[S]$, one could switch the coordinate axis to accessible substrate concentration $\alpha[S]$, where α is a substrate accessibility factor representing the substrate fraction accessible to enzymes. In eq 3, replacing $[S]$ by $\alpha[S]$ is algebraically equivalent to replacing K_m by K_m/α. Therefore, K_m is inversely proportional to substrate accessibility or, equivalently, K_m^{-1} scales in proportion to substrate accessibility.

The aforementioned factor α is henceforth abandoned because it is not experimentally available. The analysis follows with K_m^{-1}, which is proportional to α and can be derived from fitting with eq 3. By stating this proportionality, we imply that other factors (such as enzyme–substrate affinity) contribute to K_m^{-1}; however, with the other factors kept constant, K_m^{-1} is a direct measure of accessibility. In this sense, the product $K_m^{-1}[S]$ is proportional to accessible substrate concentration.

3.4. Activities Reduced to K_m^{-1}. Data in Figure 5a,b were fitted by eq 3. Results from jointly fitting MCC and MAV groups are shown in Figure 6a, while results from separate fitting of these groups are shown in Figure 6b. The product

dx.doi.org/10.1021/jp3021744 | J. Phys. Chem. B 2012, 116, 6128–6136

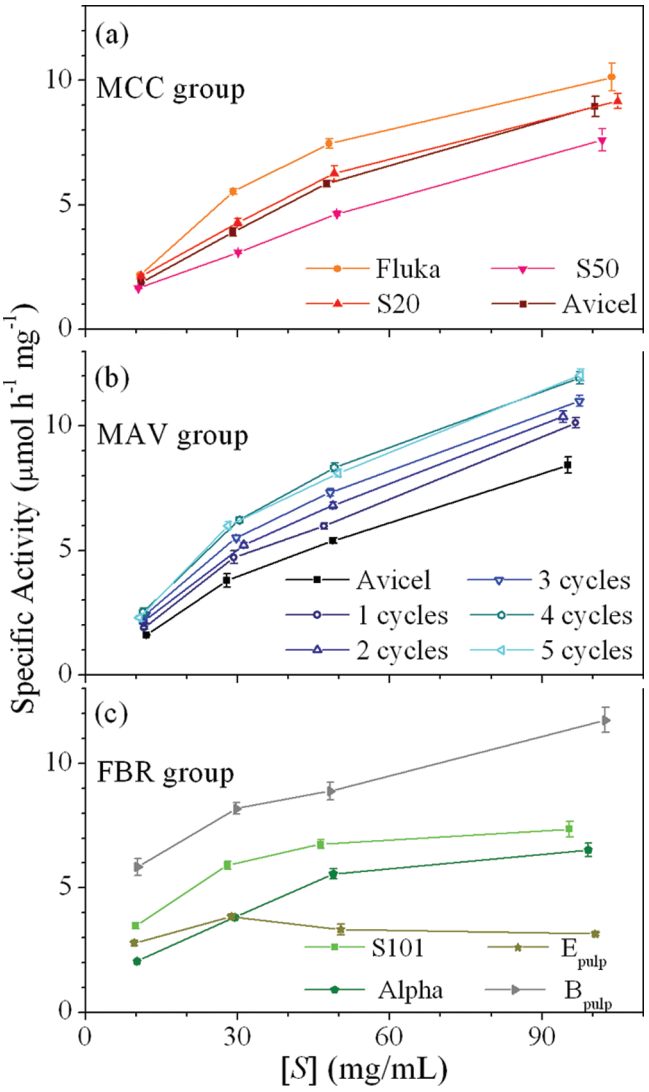

Figure 5. Specific enzymatic activity vs substrate concentration [*S*] for substrates from (a) MCC, (b) MAV, and (c) FBR groups.

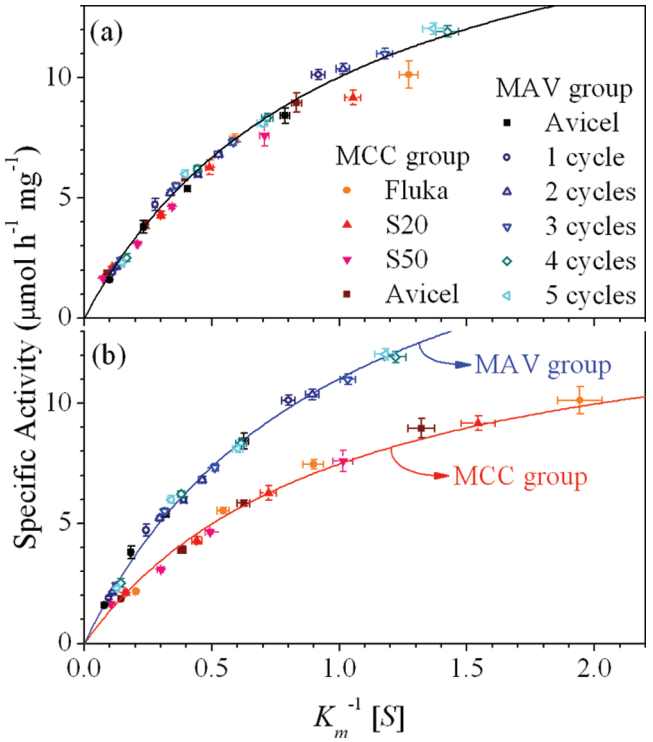

Figure 6. Specific enzymatic activity as a function of substrate concentration [*S*] multiplied by the K_m^{-1} coefficients that reduce a set of substrates to a single fit. Substrates from MCC and MAV groups were fitted (a) together or (b) separated from each other.

Table 3. K_m and k_{cat} Coefficients Derived from Fitting Specific Activity vs Substrate Concentration

		substrate K_m (mg/mL) and group k_{cat} (μmol h^{-1} mg^{-1})	
group	substrate	joint MCC and MAV fitting	separated MCC and MAV fitting
MCC	all MCC (k_{cat})	20.1 ± 0.4	15.0 ± 0.5
	Fluka	82 ± 2	53 ± 2
	S20	100 ± 3	68 ± 3
	S50	144 ± 4	100 ± 4
	Avicel	121 ± 3	76 ± 3
MAV	all MAV (k_{cat})	20.1 ± 0.4	22.1 ± 0.5
	Avicel	121 ± 3	152 ± 5
	1 cycle	105 ± 3	121 ± 4
	2 cycles	93 ± 2	105 ± 3
	3 cycles	83 ± 2	94 ± 3
	4 cycles	68 ± 2	80 ± 3
	5 cycles	71 ± 2	83 ± 3

K_m^{-1} [*S*] (abscissa of Figure 6) collapses different substrates on a single curve. Fitting quality is satisfactory, considering the simplicity of eq 3 and assumption of constant k_{cat}. (The constant k_{cat} is justifiable from the similar XRD parameters within MCC and MAV substrates.) Parameters derived from these fits are presented in Table 3. This analysis was restricted to substrates from MCC and MAV groups because including substrates from the FBR group lead to inadequate fits.

Derived K_m parameters differ when fitting MCC and MAV groups together or separated (see Table 2), but proportions between K_m^{-1} are preserved. This is because K_m^{-1} is, first of all, the multiplier of [*S*] that collapses a group of substrates into a single line, as in Figure 6. Actually, analysis could be performed with any other realistic mathematical function instead of eq 3, and still similar proportions would be derived for the multipliers of [*S*].

By jointly fitting MCC and MAV substrates (results in Figure 6a), differences in activity are forced to appear as differences in K_m. Derived K_m^{-1} (from Table 3) are shown as a function of geometric areas (Figure 7). Substrates from MCC group present increasing K_m^{-1} with increasing geometric areas. Red lines in Figure 7 are linear fits to this MCC data. The areas under red lines are divided in yellow triangles (above *y*-intercept) and gray rectangles (below *y*-intercept). The yellow triangles presumably correspond to accessibility (K_m^{-1}) contribution from external (geometric) areas, while the gray rectangle presumably correspond to accessibility contributions from pore areas, which are constant across the MCC and MAV sets (see Table 2). The key role of substrate accessibility had also been recognized based on accessibility measurements by protein adsorption.[38,39]

Sequential Avicel milling (MAV group) gradually increases K_m^{-1} as well as surface areas. However, K_m^{-1} increases beyond the yellow triangle derived from nonmilled MCC (see Figure 7). This extra K_m^{-1} is attributed to decrystallization and crystal

dx.doi.org/10.1021/jp3021744 | J. Phys. Chem. B 2012, 116, 6128–6136

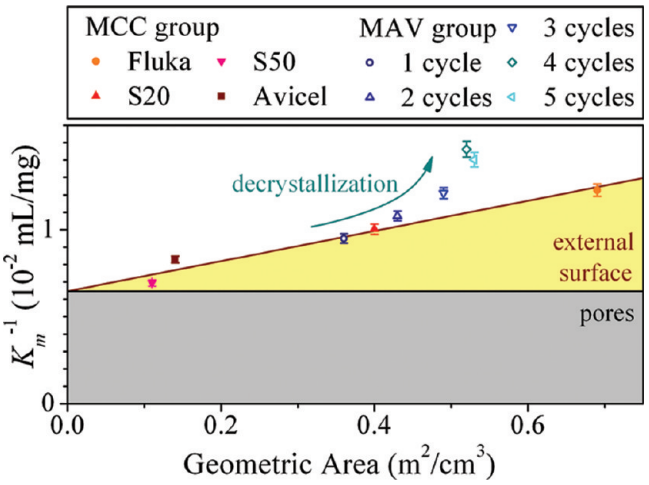

Figure 7. Coefficient K_m^{-1} (proportional to substrate accessibility) as a function of geometric surface area. K_m coefficients are those determined by jointly fitting enzymatic activities in MCC and MAV substrates, as shown in Figure 6a. Suggested contributions to accessibility (from external surfaces, pores, and decrystallization) are indicated.

thinning promoted by milling (see XRD parameters in Table 2).

In summary, by forcing activity differences to appear in one single parameter (K_m^{-1}), contributions from geometric particle areas, pore areas, and decrystallization could be discriminated. These contributions present comparable magnitudes (see Figure 7), implying that all these substrate parameters must be jointly accounted to explain EglA activity.

3.5. Sites of Endoglucanase Action. As mentioned in the introduction, the paradigm of endoglucanase activity is that it randomly hydrolyzes β-1,4 bonds in cellulose amorphous regions.[4,5] This view faces two major problems. First, by analyzing supernatants of hydrolysis (by DNS, HPAE, or other methods), endoglucanase activity is only detectable when soluble (up to six sugar units) cellodextrins are released. Release of soluble cellodextrins requires action near chain ends, i.e., not at random position. (For an alternative method that quantifies reducing ends in the solid state, see ref 34.) Second, amorphous cellulose can be in at least two competing arrangements: (i) spatially extended amorphous domains or (ii) disordered cellulose chains at crystal surfaces.[40,41] In our data, crystallinity (Table 2) significantly below cellulose contents (Table 1) indicates the presence of noncrystalline cellulose (with possible exception of E_{pulp}). However, extended amorphous domains and disordered surface chains are neither discriminated by XRD nor by other analytical techniques that probe disordered celluloses.[42,43]

A distinguished study[44] on the presence of amorphous domains employed neutron scattering of deuterated samples, electron microscopy, acid hydrolysis, and analysis of degree of polymerization. It concluded that cellulose microfibrils (in ramie) have periodic amorphous domains, with 4−5 disordered residues every 300 residues. These disordered residues, corresponding to ∼1.5% of cellulose mass, are the first to be removed by acid hydrolysis, bringing cellulose to a leveling-off degree of polymerization (∼300 residues). On the basis of these figures, endoglucanase action in amorphous domains would release a maximum of 4−5 sugar residues. Moreover, microcrystalline celluloses, which are products of acid hydrolysis, would lack extended amorphous domains, implying disordered cellulose integrally at crystal surfaces.

A new descriptive challenge emerges from this view of amorphous cellulose: how can endoglucanase act at crystal surfaces? Endoglucanase action requires cellulose chain entrance into enzyme cleft, so as to reach the active site. If the chain is adhered to the crystal, the chain must be somehow lifted to enter enzyme cleft. Lifting a cellulose chain in a random position would initially stretch the chain and ultimately require chain reconfiguration at the crystal surface, maybe through chain sliding. Referenced to the lifted position, at least one side of the chain would need to completely reconfigure (slide) at the crystal surface. The closer the lifted position is from chain ends, the smaller is the required reconfiguration. This allows us to speculate that cellulose detachment from crystals (and EglA action thereat) more likely occurs near chain ends. The preferential release of small sugars (glucose and cellobiose; see Figure 4) supports EglA activity near chain ends.

In summary, the exact site of endoglucanase action is unknown. Nevertheless, on the basis of cellulose supramolecular organization, it is feasible that endoglucanase acts primarily on disordered cellulose adhered to crystal surfaces. In this case, cellulose chain detachment from the crystal surface is necessary, and such detachment more likely occurs near chain ends. This view inferred from the structure of insoluble cellulose contradicts endoglucanase action at a random position along the chain, which has been inferred from enzyme structure as well as from activity on soluble cellulose analogues.[4,5,45,46]

3.6. Beyond K_m^{-1} Accessibility. Previous sections presented two requirements for EglA action. The first requirement is accessibility to cellulose mass, as represented by K_m^{-1} (proportional to substrate accessibility). Such accessibility is presumably represented by physical parameters like external particle areas and pore areas, and our analysis based on K_m^{-1} is summarized in Figure 7. The second requirement is cellulose chain reaching the enzyme active site, which is related to cellulose organization in a smaller scale. As discussed below, our results suggest that reachability of the active site also relates to crystallinity and crystal width. (Note that crystal width is inversely related to crystal specific surface, where disordered cellulose is supposed to exist.)

Separate MAV and MCC fit (Figure 6b) yields higher k_{cat} for MAV group than for MCC group (see Table 3). Similar difference in k_{cat} is suggested by the joint MCC and MAV fit (Figure 6a); MAV substrates tend to be above the joint fitting line, whereas MCC tend to be below it. These observations suggest higher k_{cat} due to milling-induced decrystallization and crystal thinning. In line with these observations, on E_{pulp} (highly crystalline cellulose, as inferred from composition in Table 1 compared to crystallinity in Table 2) activity reaches a maximum at k_{cat} = 2−3 μmol h^{-1} mg^{-1} (see Figure 5c). This activity is very below k_{cat} from less-crystalline celluloses (see Table 3 and Figure 5c). In the Michaelis−Menten framework, k_{cat} is the rate of product formation from enzyme−substrate complexes. One suggests that lower crystallinity (and crystal width) speeds up product formation because chain penetration into EglA is eased.

Easier chain penetration into EglA may also explain differences in the size of released sugars. Within the FBR group, the ratio between glucose + cellobiose and total reducing sugars (data of Figure 4) correlates positively with crystallinity (r = 0.86) and crystal width (r = 0.96), where r is

dx.doi.org/10.1021/jp3021744 | J. Phys. Chem. B 2012, 116, 6128−6136

the Pearson correlation coefficient. That is, longer cellulose fragments are released from less organized cellulose.

4. CONCLUSIONS

The activity of a hyperthermophilic endo-1,4-beta-glucanase from *Pyrococcus furiosus* was evaluated on 13 insoluble cellulosic substrates, including as-received and milled microcrystalline celluloses, as well as fibers with significant xylan contents. In addition to substrate composition, several substrate physical parameters were measured: particle size (and associated external particle area), wet porosity (and associated pore area), crystallinity, and crystal width. Influences of substrate properties on endoglucanase activity were investigated in the framework of Michaelis–Menten kinetics. K_m and k_{cat} coefficients were reinterpreted in the context of insoluble cellulosic substrates.

In general, enzymatic activity correlated positively with surface areas, and negatively with crystallinity and crystal width. For a set of as-received and milled microcrystalline celluloses, differences in activity could be expressed as differences in K_m^{-1}, shown to proportionally represent substrate accessibility. With this approach, accessibility contributions from external particle areas, pore areas, and decrystallization were discriminated; their comparable magnitudes implied that these substrate properties must be jointly accounted to predict endoglucanase activity.

Finally, the sites of endoglucanase action were discussed, contradicting random attack within amorphous regions. It was argued that noncrystalline cellulose is primarily adhered to crystal surfaces. This configuration restrains chain entrance into enzyme cleft and likely favors action near chain ends. Supporting this view, there was preferential release of short cellulose fragments, with longer fragments (and higher k_{cat}) observed in less-crystalline celluloses.

■ ASSOCIATED CONTENT

Supporting Information

Michaelis–Menten equation derived from the Langmuir equation under the condition of low enzyme–substrate affinity; this limit case shown to apply to the experimental conditions of the present work. This material is available free of charge via the Internet at http://pubs.acs.org.

■ AUTHOR INFORMATION

Corresponding Author

*Phone: +55 19 3518 3180. Fax: +55 19 3518 3164. E-mail: carlos.driemeier@bioetanol.org.br.

Notes

The authors declare no competing financial interest.

■ ACKNOWLEDGMENTS

Research supported by PNPD (project 560489/2010-2), FAPESP (projects 08/58037-9 and 2010/05523-3), and by LNNano, LNLS, and LNBio (proposals SEM-LV 11507 and GAR 12392).

■ REFERENCES

(1) Himmel, M. E.; Ding, S.-Y.; Johnson, D. K.; Adney, W. S.; Nimlos, M. R.; Brady, J. W.; Foust, T. D. *Science* **2007**, *315*, 804–807.
(2) Lynd, L. R.; Laser, M. S.; Bransby, D.; Dale, B. E.; Davison, B.; Hamilton, R.; Himmel, M.; Keller, M.; McMillan, J. D.; Sheehan, J.; Wyman, C. E. *Nat. Biotechnol.* **2008**, *26*, 169–172.
(3) Cortez, L. A. B., Ed. *Sugarcane Bioethanol: R&D for Productivity and Sustainability*; Blucher: São Paulo, Brazil, 2010.
(4) Béguin, P.; Aubert, J. P. *FEMS Microbiol. Rev.* **1994**, *13*, 25–58.
(5) Lynd, L. R.; Weimer, P. J.; Van Zyl, W. H.; Pretorius, I. S. *Microbiol. Mol. Biol. Rev.* **2002**, *66*, 506–577.
(6) Zhang, Y.-H. P.; Lynd, L. R. *Biotechnol. Bioeng.* **2004**, *88*, 797–824.
(7) Mansfield, S. D.; Mooney, C.; Saddler, J. N. *Biotechnol. Prog.* **1999**, *15*, 804–816.
(8) Henning, J.; Kristensen, J. B.; Felby, C. *Biofuels, Bioprod. Biorefin.* **2007**, *1*, 119–134.
(9) Bhat, M. K. *Biotechnol. Adv.* **2000**, *18*, 355–383.
(10) Jeoh, T.; Ishizawa, C. I.; Davis, M. F.; Himmel, M. E.; Adney, W. S.; Johnson, D. K. *Biotechnol. Bioeng.* **2007**, *98*, 112–122.
(11) Arantes, V.; Saddler, J. N. *Biotechnol. Biofuels* **2010**, *3*, 4.
(12) Grethlein, H. E. *Nat. Biotechnol.* **1985**, *3*, 155–160.
(13) Gama, F. M.; Teixeira, J. A.; Mota, M. *Biotechnol. Bioeng.* **1994**, *43*, 381–387.
(14) Ishizawa, C. I.; Davis, M. F.; Schell, D. F.; Johnson, D. K. *J. Agric. Food Chem.* **2007**, *55*, 2575–2581.
(15) Hall, M.; Bansal, P.; Lee, J. H.; Realff, M. J.; Bommarius, A. S. *FEBS J.* **2010**, *277*, 1571–1582.
(16) Park, S.; Baker, J. O.; Himmel, M. E.; Parilla, P. A.; Johnson, D. K. *Biotechnol. Biofuels* **2010**, *3*, 10.
(17) Driemeier, C.; Calligaris, G. A. *J. Appl. Crystallogr.* **2011**, *44*, 184–192.
(18) Bauer, M. W.; Driskill, L. E.; Callen, W.; Snead, M. A.; Mathur, E. J.; Kelly, R. M. *J. Bacteriol.* **1999**, *181*, 284–290.
(19) Wang, H.; Squina, F.; Segato, F.; Mort, A.; Lee, D.; Pappan, K.; Prade, R. *Appl. Environ. Microbiol.* **2011**, *77*, 5199–5206.
(20) ASTM E1758–01: *Standard Test Method for Determination of Carbohydrates in Biomass by High Performance Liquid Chromatography*; American Society for Testing and Materials: West Conshohocken, PA, 2001.
(21) Driemeier, C.; Oliveira, M. M.; Mendes, F. M.; Gómez, E. O. *Powder Technol.* **2011**, *214*, 111–116.
(22) Driemeier, C.; Mendes, F. M.; Oliveira, M. M. *Cellulose* **2012**, submitted for publication.
(23) Park, S.; Venditti, R. A.; Jameel, H.; Pawlak, J. J. *Carbohydr. Polym.* **2006**, *66*, 97–103.
(24) Driemeier, C.; Pimenta, M. T. B.; Rocha, G. J. M.; Oliveira, M. M.; Mello, D. B.; Maziero, P.; Gonçalves, A. R. *Cellulose* **2011**, *18*, 1509–1519.
(25) Lutterotti, L.; Matthies, S.; Wenk, H.-R.; Schultz, A. S.; Richardson, J. W., Jr. *J. Appl. Phys.* **1997**, *81*, 594–600.
(26) CAZy: Carbohydrate Active Enzymes. www.cazy.org.
(27) Squina, F. M.; Santos, C. R.; Ribeiro, D. A.; Cota-Silva, J.; de Oliveira, R. R.; Ruller, R.; Mort, A.; Murakami, M. T.; Prade, R. A. *Biochem. Biophys. Res. Commun.* **2010**, *399*, 505–511.
(28) Bradford, M. M. *Anal. Biochem.* **1976**, *72*, 248–254.
(29) ExPASy: SIB Bioinformatics Resource Portal. www.expasy.org.
(30) Cheng, Y. S.; Ko, T. P.; Wu, T. H.; Ma, Y.; Huang, C. H.; Lai, H. L.; Wang, A. H.; Liu, J. R.; Guo, R. T. *Proteins* **2011**, *74*, 1193–204.
(31) McIlvaine, T. C. *J. Biol. Chem.* **1921**, *49*, 183–186.
(32) Miller, G. L. *Anal. Chem.* **1959**, *31*, 426–428.
(33) Michaelis, L.; Menten, M. L. *Biochem. Z.* **1913**, *49*, 333–69.
(34) Kongruang, S.; Han, M. J.; Breton, C. I. G.; Penner, M. H. *Appl. Biochem. Biotechnol.* **2004**, *113*, 213–231.
(35) Zhang, Y.-H. P.; Lynd, L. R. *Biomacromolecules* **2005**, *6*, 1510–1515.
(36) Okazaki, M.; Moo-Young, M. *Biotechnol. Bioeng.* **1978**, *20*, 637–663.
(37) Zhang, Y.-H. P.; Lynd, L. R. *Biotechnol. Bioeng.* **2006**, *94*, 888–898.
(38) Hong, J.; Ye, X.; Zhang, Y.-H. P. *Langmuir* **2007**, *23*, 12535–12540.
(39) Wang, Q. Q.; He, Z.; Zhu, Z.; Zhang, Y.-H. P.; Ni, Y.; Luo, X. L.; Zhu, J. Y. *Biotechnol. Bioeng.* **2012**, *109*, 381–389.
(40) Engström, A.-C.; Ek, M.; Henriksson, G. *Biomacromolecules* **2006**, *7*, 2027–2031.
(41) Nishiyama, Y. *J. Wood Sci.* **2009**, *55*, 241–249.

(42) Wickholm, K.; Larsson, P. T.; Iversen, T. *Carbohydr. Res.* **1998**, *312*, 123−129.
(43) Müller, M.; Czihak, C.; Schober, H.; Nishiyama, Y.; Vogl, G. *Macromolecules* **2000**, *33*, 1834−1840.
(44) Nishiyama, Y.; Kim, U.-J.; Kim, D.-Y.; Katsumata, K. S.; May, R. P.; Langan, P. *Biomacromolecules* **2003**, *4*, 1013−1017.
(45) Reese, E. T.; Siu, R. G. H.; Levinson, H. S. *J. Bacteriol.* **1950**, *59*, 485−497.
(46) Kleywegt, G. J.; Zou, J.-Y.; Divne, C.; Davies, G. J.; Sinning, I.; Stahlberg, J.; Reinikainen, T.; Srisodsuk, M.; Teeri, T. T.; Jones, T. A. *J. Mol. Biol.* **1997**, *272*, 383−397.